Strain and stress build-up in He-implanted UO 2 single crystals: an X-ray diffraction study

Aurélien Debelle, Alexandre Boulle, Frederico Garrido, Lionel Thomé

Strain and stress build-up in He-implanted UO_2 single crystals: an X-ray diffraction study

Aurélien Debelle[a], Alexandre Boulle[b], Frédérico Garrido[a], Lionel Thomé[a]

a. Centre de Spectrométrie Nucléaire et de Spectrométrie de Masse (CSNSM - UMR 8609), CNRS-IN2P3-Univ. Paris-Sud - Bâtiment 108 - 91405 Orsay Cedex, France
b. Science des Procédés Céramiques et de Traitements de Surface CNRS UMR 6638, Centre Européen de la Céramique, 12 rue Atlantis, 87068 Limoges, France

Abstract

The strain and stress build-up in 20-keV He-implanted UO_2 single crystals have been determined by means of X-ray diffraction through reciprocal space mapping, with the use of a model dedicated to the analysis of the strain/stress state of ion-irradiated materials. Results indicate that the undamaged part of the crystals exhibits no strain or stress; on the other hand, the implanted layer undergoes a tensile strain directed along the normal to the surface of the crystals and a compressive in-plane stress. The build-up of both strain and stress with He fluence exhibits a two-step process: (i) a progressive increase up to a maximum level of ~ 1% for the strain and ~ -2.8 GPa for the stress, followed by (ii) a dramatic decrease. The origin of the strain and stress build-up is the formation of both self-interstitial defects and small He-vacancy clusters. The strain, and stress relief is tentatively attributed to the formation of extended defects (such as dislocations) that induce a plastic relaxation.

Keywords: XRD; UO_2; radiation effects; elastic strain; He; defects;

PACS: 61.05.cp; 61.80.Jh; 61.72.J-; 61.72.Dd; 62.20.D-

Introduction

During the storage over long-term periods of spent nuclear fuels, one of the main issues lies in the ability of the waste form, submitted to several irradiation sources which may influence its macroscopic stability, to efficiently confine the radioactive elements. Spent fuel is mainly composed of uranium dioxide UO_2 (urania) into which actinides and fission fragments are present. Both uranium isotopes and actinides are unstable elements that undergo alpha decay. This phenomenon leads to the production of both low-energy heavy nuclei (alpha recoils) and high-energy alpha particles, and it is the primary damaging source in nuclear waste solids. The alpha recoils are responsible for crystal damage through elastic collisions. Alpha particles have a weak irradiation impact (only a few atomic displacements), but their concentration can reach high levels, more than 1 at.% over long storage periods, and it is well known that He is almost insoluble in the fuel lattice: the formation of He-vacancy complexes and even He bubbles has already been predicted by calculations [1] and experimentally observed [see e.g. 2-5]. Since urania is a crystalline compound, elastic strain and stress are likely to develop upon this self-irradiation, and the issue of their influence on the overall structural stability of the material is thus raised. Answering this question requires a complete and accurate characterization of the strain/stress state of UO_2 upon irradiation.

Recently, Garrido *et. al.* determined, by Rutherford backscattering spectrometry and Channelling (RBS/C), the disordering build-up in UO_2 single crystals (SCs) submitted to 20-keV He ion implantation at room temperature (RT) [5]. It was found that this disordering kinetics follows a two-step behaviour (for the reader convenience, these results are displayed in Fig. 3(c), together with the present XRD data), and that the relevant key parameter is the He concentration which triggers the formation of He bubbles. The work presented in the current paper aims at determining, by means of high-resolution X-ray diffraction (HRXRD) through reciprocal space maps (RSMs), both the strain and stress states of UO_2 SCs submitted

to He implantation. Emphasis is put on the first step of the disordering build-up determined by RBS/C, *i.e.* up to the very beginning of the formation (or rather, the observation by TEM, see [5]) of He bubbles. It is worth mentioning that this study, although fundamental since it investigates a model system (pure UO_2 SCs), provides basic data relevant for modelling and predicting the behaviour of the fuel under long-term interim storage.

II Experimental details

II.1. Crystal preparation and ion implantation

The specimens used in this study are mirror-polished (100)-oriented UO_2 single crystals possessing the fluorite-type structure ($Fm\bar{3}m$) and a lattice parameter $a_0 = 0.547$ nm. The crystals were annealed at 1400 °C under Ar/H_2 atmosphere in order to fix the stoichiometric composition of O/U = 2:1 (as verified by RBS and channelling measurements) and to remove any polishing damage. Subsequently, RT implantations were performed with the IRMA implantor of the CSNSM-Orsay with 20-keV He ions at fluences ranging from $5x10^{14}$ to $5x10^{16}$ cm^{-2}. For all implantation fluences, the ion flux was kept below a few 10^{12} $cm^{-2}.s^{-1}$. Consequently, the temperature of the sample never exceeded a few tens of degrees, which is lower than the temperature (300°C) where the first annealing stage has been observed [6], and well below the temperature for He migration (~600°C, see e.g. [2]). Hence, no flux effect is expected in the present implantation conditions. Note that an incident beam angle of 7° was used during implantation to avoid any channelling phenomenon. Monte Carlo simulations using the SRIM code [7] were run in order to determine the corresponding mean projected range (and range straggling), R_p ~ 94 nm (ΔR_p~46 nm), the helium depth profile and the damage level expressed in displacements per atom (dpa). Threshold displacement energies

were assumed to be 40 eV and of 20 eV for U and O atoms respectively [8]. It must be mentioned that, although the electronic energy loss is, at the beginning of the slowing down process of 20-keV He ions, 10 times higher (~0.1 keV.nm^{-1}) than the nuclear energy loss, it does not have any influence on the UO_2 crystalline structure since its magnitude is much lower than the threshold value to induce any significant effect in this material (see e.g. [9]).

II.2. XRD measurements

The crystals were characterized by HRXRD using a laboratory diffractometer equipped with a rotating Cu anode, a four-reflection monochromator and a curved position sensitive detector (for a detailed description of the set-up, see e.g. [10]). The X-ray beam used to characterise the samples was monochromatic (Cu Kα_1, $\Delta\lambda/\lambda=1.4\times10^{-4}$) and parallel in the detector plane ($\Delta\theta$ = 12 arcsec). A five-movement sample holder allowed precise positioning of the single crystals. The formalism used in this paper is the one presented in [11], which is based on the work of Dederichs with regard to the treatment of diffuse X-ray scattering [12]: (i) K_N and $K_{//}$ are the normal (out-of-plane) and parallel (in-plane) components of the scattering vector K ($2sin\theta/\lambda$), respectively; (ii) $H_{(400)}$ refers to the reciprocal lattice vector for the (400) reflection; (iii) q_N is defined as K_N-$H_{(400)}$ and represents the deviation from the reciprocal lattice vector (sometimes called reduced scattering vector). Reciprocal space maps (RSMs), which display the scattered intensity in a particular (K_N,$K_{//}$) plane around a given reciprocal lattice point (RLP), have been recorded. The (400) Bragg reflection (2θ~68.567°) has been principally explored, but the (402) Bragg reflection (2θ~78.067°) has also been studied in a specific case to determine the in-plane lattice parameter. The (402) planes make a ψ-angle of 26.57° with respect to the sample surface, and in this case, measurements have been performed in an asymmetric glancing-incidence configuration with $\theta = \omega + \psi$, ω being

the incidence angle *(ω~12°)*. Note that in both cases, the thickness probed by the X-ray beam is much larger (minimum 0.9 μm with the 1/e attenuation length criterion) than the implanted layer (~200 nm). In the following, positions on the map are located by the in-plane and out-of-plane components of the scattering vector, and also by (i) ($-q_N/H_{(400)}$), which is equal - provided that deviations are weak, which is the case in the present study - to the elastic strain in the direction normal to the surface of implanted samples, and (ii) ($\Delta K_{//}/H_{(400)}$), which directly indicates the width (here in degrees) of the RLP in the transverse direction, *i.e.*, in the present case, the width of the rocking-curve.

III. Results and discussion

III.1. Reciprocal space mapping

Figure 1(a) depicts the scattered intensity (in logarithmic scale) in the vicinity of the (400) Bragg reflection for an urania SC implanted at 0.8 at.% / 0.4 dpa ($6x10^{15}$ cm^{-2}), *i.e.* at a low damage level according to the disordering build-up previously obtained by RBS/C (see [5] and Fig. 3(c)). On this RSM, a diffuse streak directed along an inclined direction with respect to the K_N axis (actually along the 2θ direction) is visible. This signal is an artifact (the 'detector streak') due to the large opening of the counting channels of the detector (~0.015°) compared to the very small beam divergence (0.0033°) [10]. More important is the strong signal – square mesh feature on the map - observed at the K_N coordinate of the unstrained (unimplanted) material, which is located at 7.3126 nm^{-1}. This intense signal is also visible on unimplanted crystals; it corresponds to the undisturbed part of the samples probed by X-rays. It is used in the following as an internal strain gauge to quantify the elastic strain. It is worth mentioning that several intense spots are visible at this K_N coordinate, which indicates that the

urania SCs used in this study are in fact multi-crystals, *i.e.* crystals composed of a few (typically two to four) large mosaic blocks with a slight disorientation angle (~0.1°, as can be seen on the map in Fig. 1(a)). These crystals must yet be considered as single crystals and not as polycrystals. Indeed, the width of the rocking-curve (see top axis of the map in Fig. 1(a)) is only ~0.05°, which indicates a good crystalline quality. This statement is also supported by the fact that RBS/C measurements carried out on these samples provide a value of $\chi_{min} \sim 0.015$ (*i.e.* very close to the theoretical value for perfect crystals). Finally, no grain boundary-like structure was observed at the surface of the specimens by scanning electron microscopy (SEM). It is finally worth mentioning that all blocks are assumed to behave similarly upon irradiation.

Also visible on the map in Fig. 1(a) is a spreading of the scattered intensity along the K_N direction in the region of higher lattice parameter (positive $-q_N/H_{(400)}$ values). This signal arises from the scattering of the X-ray beam by the implanted layer. Intensity modulations are clearly observed (see also Fig. 2 where the K_N profile extracted from the (400) RSM is represented). The presence of several "diffraction peaks" arising from the damaged layer of UO_2 SCs irradiated with 300-keV Xe ions at RT has previously been reported [13], but this feature was not explained. Actually, this fringe pattern reveals the presence of a strain depth profile which is the result of the irradiation conditions (see e.g. Refs. 14-16). An accurate determination of this strain profile requires the refinement of the experimental curves with a dynamical treatment of the XRD data (see e.g. [16]). Note that in the current study, only the maximum strain (obtained from the position, on the K_N profiles, of the last fringe in the low-value K_N range) and associated maximum stress are considered (see Figs. 3(a)-(b)). However, it is worth mentioning that, since the fringe spacing is directly related to the width of the strained region ($\Delta z = 1/\Delta K$), the strain depth distribution can be roughly reconstructed assuming a symmetric profile [17]. In the present case, it is found that the width of the strain

depth profile is much larger than that of the damage profile determined by channelling [5], but on the contrary it is consistent with that of the SRIM-predicted He depth distribution (FWHM~140 nm), as already observed in similar experiments on, e.g., cubic zirconia [18] and 6H-SiC [19].

Figure 1(b) displays the RSM recorded on the same He-implanted SC (0.8 at.% / 0.4 dpa) but around the (402) reflection. It must be pointed out that in this case, the strain is equal to $-q_N/H_{(402)}$, where $H_{(402)} = H_{(400)}*\cos\psi$. Since the scattering vector $K_{(402)}$ has both an in-plane and an out-of-plane component, the corresponding lattice parameters can be calculated. In the present case of a (100)-oriented crystal, the following expressions are used:

$$a_N = \left(\frac{\sqrt{4^2}}{K_{N_{(402)}}} \right) \text{ and } a_{//} = \left(\frac{\sqrt{2^2}}{K_{//_{(402)}}} \right)$$

From Figure 1(b), it appears that the coordinates of the maximum of the signal (square mesh feature on the map) due to the undisturbed part of the urania crystal is located at $K_N \sim 7.312$ nm^{-1} and $K_{//} \sim 3.653$ nm^{-1}. The corresponding values of the lattice parameters are nearly equal (within the error bars) to those of virgin urania. Hence, the undamaged layer does not exhibit any strain or stress, as it could have been expected from previous works on different materials (see e.g. [11,20-21]). Likewise, it is clear that the scattering vector corresponding to the implanted region shares the same $K_{//}$ component (~3.653 nm^{-1}) as the underlying layer. This result indicates the absence of in-plane deformation. On the contrary, as already seen on the (400) RSM, since the signal smears along the K_N direction, the K_N components in the undamaged and implanted regions are very different. This discrepancy confirms the presence of a tensile normal strain in the damaged layer. It is thus noteworthy that the implantation-induced strain is localized along the direction normal to the crystal surface. It should also be noticed that such a strain state corresponds to a tetragonal distortion

of the initial cubic lattice. A similar result was obtained by Speriosu in a work that aimed at characterizing the irradiation-induced strain state in He-implanted Gd, Tm, and Ga:YIG [21].

III.2. Strain/stress state analysis

A same strain state as the one determined in the present irradiated UO_2 SCs has already been observed in low-energy Cs-implanted (cubic) zirconia SCs, and the corresponding stress state has been derived with the use of a strain/stress model dedicated to ion-irradiated materials [11]. This model takes into account the reaction of the unirradiated layer (substrate) to the lattice volume change imposed by the creation of radiation-induced defects in the implanted layer. It is described by a two-step process: in the first step, radiation defects induce a positive local lattice volume change (called 'free' elastic strain) in the thin layer submitted to ion irradiation; in the second step, since the lateral dimensions imposed by the underlying substrate are fixed, the thin irradiated layer is subjected to an in-plane biaxial compressive stress $\sigma_{//}$ which totally cancels the (free) in-plane strain induced by the defects. The development of this stress results in an additional tensile-strain contribution in the opposite direction (out-of-plane strain) due to the substrate reaction (SR) by Poisson effect. This contribution is proportional to the initial free deformation and depends on the elastic constants of the material. To summarise, the total normal elastic strain, which is the one experimentally measured, is the result of two contributions: (i) a tensile elastic strain due to the formation of radiation defects, and (ii) a tensile elastic strain arising from a Poisson effect reaction owing to the substrate reaction. Considering the elastic constants of UO_2 (see below), this latter component contributes (in the (100) direction) to nearly 40% to the total measured normal strain (~33% for zirconia and ~50% for $MgAl_2O_4$). According to elasticity theory, the

relationship linking the total normal strain, $\varepsilon_N^{(tot)}$ to the in-plane stress, in the case of a (100)-oriented crystal [10], is:

$$\sigma_{//} = -\frac{C_{11}(C_{11}+C_{12}) - 2C_{12}^2}{C_{11}+2C_{12}}\varepsilon_N^{(tot)}$$

where $C_{i,j}$ are the elastic stiffnesses (we used here the following experimental values [22]: C_{11} = 396 GPa, C_{12} = 121 GPa, and C_{44} = 64 GPa).

The same strain/stress state has been observed for all crystals implanted up to the fluence of $3x10^{16}$ cm^{-2} (*i.e.* before the strain relaxation, see below and Figs. 3(a)-(b)). Hence, using the above-described model, it is possible to follow the variation of both the maximum normal strain, $\varepsilon_N^{(max)}$, and of its associated stress, $\sigma_{//}^{(max)}$, as a function of the two important parameters that are the He atomic concentration and the damage level (in dpa). The corresponding results are presented in Figs. 3(a) and (b), respectively, along with the RBS/C data (Fig. 3(c)) previously reported in [5]. The in-plane stress is compressive and it amounts to ~ -2.8 GPa for the $3x10^{16}$ cm^{-2} fluence (which corresponds to 4 at.% / 2 dpa). This stress value obviously depends on the chosen elastic constants, which can besides be modified due to the radiation damage, but it surely lies in the GPa range. This result indicates that UO_2 can withstand high stress levels. The out-of-plane strain is positive and reaches ~1%. This value is in agreement with the one (~0.84 %) found by Weber in a (relatively) similar work on UO_2 SCs alpha-irradiated at RT with a $^{238}PuO_2$ source [23]. Defects at the origin of this measured tensile strain must have a positive relaxation volume, which is the volume change of the crystal due to the distortion field of one defect. The formation of self-interstitial atoms (SIAs), created directly by ballistic collisions during the elastic slowing-down of He ions, can obviously be assumed. Since He bubbles have been observed by TEM at the end of the first step of the damage build-up (see [5]), it is most likely that in the primary implantation stage, He atoms are trapped at vacancies, forming He-vacancy (He_nV_p) complexes precursor of the

bubbles observed at higher He concentration. In addition, it is observed that the width of the strain depth profile is consistent with that of the SRIM-predicted He distribution (see III.1). Consequently, a contribution of He_nV_p complexes to the elastic-strain build-up may also be considered (as also clearly evidenced in low-energy He-implanted zirconia [18] and SiC [19]). Finally, it must be noted that the diffuse scattering observed on the RSM in Fig. 1(a) is very weak: the scattered intensity is confined to a small $K_{//}$ region, even around the reflection corresponding to the damaged layer. This result suggests that defects at the origin of the strain are of small dimension, *i.e.* no significant defect clustering occurred (at least before the strain relaxation, see below), which is consistent with the radiation conditions used here.

III.3. Strain/stress build-up

The second feature in Fig. 3 that must be put forward is the presence of a two-step strain (and stress) build-up. In the first step, it is observed a progressive increase of the elastic strain up to a maximum level reached at 4 at.% / 2 dpa ($3x10^{16}$ cm^{-2}). Conversely, in the second step, which starts between 4 at.% / 2 dpa and 6.6 at.% / 3.3 dpa ($5x10^{16}$ cm^{-2}), the elastic strain dramatically drops. Indeed, the XRD signal corresponding to the damaged layer of the crystals implanted at 6.6 at.% / 3.3 dpa appears to be noticeably different from that recorded at lower fluence. Actually, the oscillatory structure has been smoothed out and replaced by a broad diffuse-scattering-like component (see Fig. 2), revealing that the elastic strain has been relieved. However, the presence of a scattered intensity smearing towards low K_N values indicates that the irradiated layer is still characterized by an average lattice parameter which is larger than that of a virgin crystal. Variations of the stress and strain are anti-correlated, which was expected since both parameters are, in the framework of the model used here, intrinsically of opposite sign. It is noteworthy that this strain (and stress) relaxation occurs at the same fluence as the huge increase of the damage fraction measured by RBS/C

(see Fig. 3). This finding is a striking result that points out that both results are indeed related. Actually, they can both be ascribed to a microstructural transformation. It is first worth mentioning that this relaxation did not occur due to the flaking of the surface of the crystal, as checked up by SEM, nor by a fracturation of the crystal caused by the high pressure of gas bubbles, since this mechanism only arises at higher gas concentration [5,24]. It is interesting to note that, in an extensive work (see e.g. [21, 25-26]) that aimed at investigating the strain/stress state of several materials (e.g. Si, Ge, GaAs) irradiated with different ions (e.g. He, B, Ne, Si) up to amorphization, Speriosu *et al.* never observed a strain relaxation, but in some cases [26], they evidenced a saturation of the elastic strain yield. They postulated that this phenomenon should be due to (i) defect annihilation (*i.e.* dynamic annealing during implantation) at defect sinks and/or (ii) defect trapping at defect clusters. Likewise, Weber, in his work on alpha-irradiated UO_2 (which is similar to the work presented here), also observed the saturation of the elastic strain [23]. This saturation phenomenon was well reproduced with an in-growth defect model that takes into account both defect production and (dynamic) defect-annealing, and for which creation and annihilation dose rates become equal at high fluences. However, this model is valid as long as no significant defect clustering occurs, *i.e.* as long as no defect precipitation into new, extended defects takes place. Indeed, the effect of extended defects (such as dislocations) on the stability of a crystalline lattice is noticeably different from that of point-defect clusters, especially in terms of strain field. It has been shown that, at a given fluence, if the irradiated layer remains crystalline, the deposited energy during irradiation can go into the formation of dislocations whose density and size increase with the fluence [26,28]. Then, in this fluence range, the irradiated layer does not anymore respond elastically to the radiation damage but becomes plastically deformed, which induces a relaxation of the elastic strain (it becomes energetically favourable to decrease the macroscopic homogeneous strain at the expense of creating heterogeneous localized

distortions, as frequently observed in lattice-mismatch epitaxial layers). The formation of extended defects at high fluence in the current study would be consistent with the XRD data. The fact that this strain relaxation did not occur in Weber's study while it is observed in the present one suggests a different behaviour of point defects in the two cases. Point-defect trapping, migration and recombination are the most important mechanisms responsible for strain variation, and it is known that implanted inert-gas atoms can act as strong trapping sites for point defects, particularly for interstitials. The main difference between the two studies lies in the He concentration: in Weber's work the maximum He concentration was estimated to be ~0.08%, while in the current one it reaches ~4 at.% when the strain relaxation occurs. Therefore, the presence of a large He concentration in the present study may inhibit defect migration (hence annihilation), leading to a defect clustering phenomenon and then to defect precipitation into extended defects. In ion-irradiated zirconia, a material that shares many similarities with urania, a strain relaxation was also observed and it was demonstrated that it resulted from the clustering of SIAs into dislocation loops [27-29]. It is interesting to note that this scenario of defect re-organization was also proposed in works which aimed at investigating the lattice parameter changes in the fuel submitted to burn-up levels over a very broad range (for a detailed review, see [30]) and where, surprisingly, a similar two-step process was observed. Consequently, it is assumed that the most likely mechanism to account for the strain (and stress) relaxation observed in the present study is the formation of extended defects such as dislocations and dislocation loops, this process being enhanced by the presence of He acting as trapping sites for point defects.

Conclusion

The strain and stress states of UO_2 single crystals submitted to low-energy (20-keV) He implantation have been investigated by means of X-ray diffraction with the use of a model dedicated to the analysis of the strain/stress state of ion-irradiated materials. It is found that the undamaged part of the crystals exhibits no strain or stress. On the contrary, the implanted part undergoes a tensile strain directed along the normal to the surface of the crystal and a compressive in-plane stress. The formation of radiation-induced self-interstitial defects and of small He-vacancy complexes is at the origin of the strain and stress build-up. Both strain and stress magnitudes increase as a function of helium fluence until high levels are reached (~ 1% for the strain and ~ -2.8 GPa for the stress). Then, a relaxation of the elastic strain is observed. The formation of extended defects arising from a self-reorganization process of interstitial defect clusters and inducing a plastic relaxation appears to be the most likely mechanism to account for this strain relief. More work is needed to confirm this assumption, especially RSMs measurements at He concentration above the strain relaxation and transmission electron microscopy to image the radiation-induced defects, but such experiments are difficult to carry out in the case of nuclear and radioactive materials such as UO_2.

Finally, these results show that the presented methodology, already implemented in 'regular' materials, can successfully be used in UO_2, a material which is of particular interest as it is a key constituent of nuclear fuel assemblies. In addition, this study provides basic data for the understanding and modelling of the damaging mechanisms in nuclear fuel under long-term interim storage conditions.

Acknowledgements

Ion implantation was performed with the IRMA implantor of the CSNSM-Orsay, and we are thus grateful to the Semiramis staff for their help during these implantations. This study is supported by the *Programme sur l'Aval du Cycle et l'Energie Nucléaire (PACEN)*, and it was partially financed by the "Groupement National de Recherche" (GNR) MATINEX.

References

[1] Yun Y, Eriksson O, Oppeneer PM (2009) Journal of Nuclear Materials 385:510

[2] Guilbert S, Sauvage T, Garcia P, Carlot G, Barthe MF, Desgardin P, Blondiaux G, Corbel C, Piron JP, Gras JM (2004) Journal of Nuclear Materials 327:88

[3] Sattonnay G, Garrido F, Thomé L (2004) Philosophical Magazine Letter 84:109

[4] Sattonnay G, Vincent L, Garrido F, Thomé L (2006) Journal of Nuclear Materials 355:131

[5] Garrido F, Vincent L, Nowicki L, Sattonnay G, Thomé L (2008) Nuclear Instruments and Methods in Physics Research Section B: Beam Interactions with Materials and Atoms 266:2842

[6] Weber W J (1983) Journal of Nuclear Materials 114:213

[7] Ziegler J F, Biersack J P, Littmark U (1985) The Stopping and Range of Ions in Solids. Pergamon, New York. SRIM program can be downloaded at: www.srim.org.

[8] Soullard J (1985) Journal of Nuclear Materials 135:190

[9] Matzke H, Lucuta PG, Wiss T (2000) Nuclear Instruments and Methods in Physics Research Section B: Beam Interactions with Materials and Atoms 166-167:920

[10] Boulle A, Masson O, Guinebretière R, Lecomte A, Dauger A (2002) Journal of Applied Crystallography 35:606

[11] Debelle A, Declémy A (2010) Nuclear Instruments and Methods in Physics Research Section B: Beam Interactions with Materials and Atoms 268:1460

[12] Dederichs P H (1973) Journal of Physics F: Metal Physics 3:471

[13] Matzke H, Turos A, Linker G (1994) Nuclear Instruments and Methods in Physics Research Section B: Beam Interactions with Materials and Atoms 91:294

[14] Emoto T, Ghatak J, Satyam P V, Akimoto K (2009) Journal of Applied Physics 106:043516

[15] Debelle A, Declémy A, Vincent L, Garrido F, Thomé L (2009) Journal of Nuclear Materials 396:240

[16] Boulle A, Debelle A (2010) Journal of Applied Crystallography 43:1046

[17] Sousbie N, Capello L, Eymery J, Lagahe Ch, Rieutord F (2006) Journal of Applied Physics 99:103509

[18] Velisa G, Debelle A, Vincent L, Thomé L, Declémy A, Pantelica D (2010) Journal of Nuclear Materials 402:87

[19] Leclerc S, Beaufort M F, Declémy A, Barbot J F (2008) Applied Physics Letters 93:122101

[20] Rao S I, Houska C R (1990) Journal of Materials Science 25:2822

[21] Speriosu V S (1981) Journal of Applied Physics 52:6094

[22] Wachtman Jr JB, Wheat ML, Anderson HJ, Bates JL (1965) Journal of Nuclear Materials 16:39

[23] Weber WJ (1981) Journal of Nuclear Materials 98:206

[24] Matzke Hj (1992) Journal of Nuclear Materials 189:141

[25] MacNeal B E, Speriosu V S (1981) Journal of Applied Physics 59:3235

[26] Speriosu V S, Paine B M, Nicolet M-A, Glass H L (1982) Applied Physics Letters 40:604

[27] Sickafus K E, Matzke Hj, Hartmann Th, Yasuda K, Valdez J A, Chodak P III, Nastasi M, Verall R A (1999) Journal of Nuclear Materials 274:66

[28] Moll S, Thomé L, Sattonnay G, Debelle A, Vincent L, Garrido F, Jagielski J (2009) Journal of Applied Physics 106:073509

[29] Debelle A, Moll S, Décamps B, Thomé L, Sattonnay G, Garrido F, Jozwik I, Jagielski J (2010) Scripta Materialia 63:665

[30] Spino J, Papaioannou D (2000) Journal of Nuclear Materials 281:146

Figure captions

Figure 1: Reciprocal space maps in the vicinity of (a) the (400) Bragg reflection and (b) the (402) Bragg reflection of a UO_2 single crystal implanted with He at 0.8 at.% / 0.4 dpa ($6x10^{15}$ cm^{-2}). The intensity is in logarithmic scale. Definition of the different axes is given in the text.

Figure 2: K_N profiles extracted from (400) RSMs recorded on UO_2 single crystals implanted with He at 0.8 at.% / 0.4 dpa ($6x10^{15}$ cm^{-2}) and 6.6 at.% / 3.3 dpa ($5x10^{16}$ cm^{-2}).

Figure 3: Variation as a function of both the He atomic concentration and the damage dose (expressed in dpa) of (a) the maximum elastic normal strain (ε_N^{max}), and (b) the maximum in-plane biaxial stress ($\sigma_{//}^{max}$) exhibited by the UO_2 implanted layer. The size of the symbols corresponds to the error bar. Solid and dashed lines are guides to the eyes. The damage build-up determined by RBS/C for the U sublattice is displayed in (c).

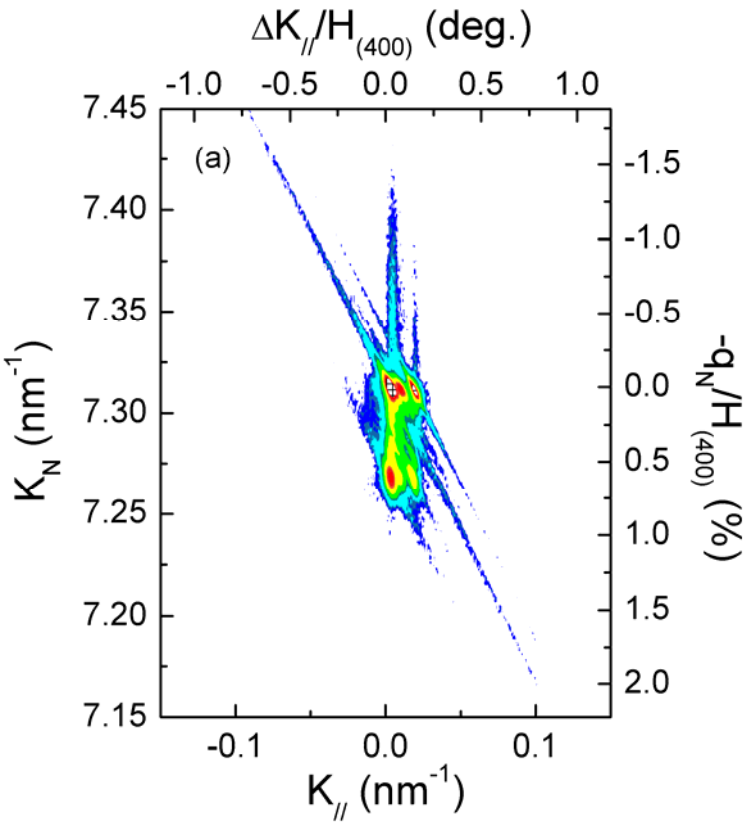
ΔK//H(400) (deg.)
-1.0
-0.5
0.0
0.5
1.0
(a)
7.45
7.40
7.35
7.30
7.25
7.20
7.15
KN (nm-1)
-1.5
-1.0
-0.5
0.0
0.5
1.0
1.5
2.0
-qN/H(400) (%)
-0.1
0.0
0.1
K// (nm-1)

Figure 1(a)

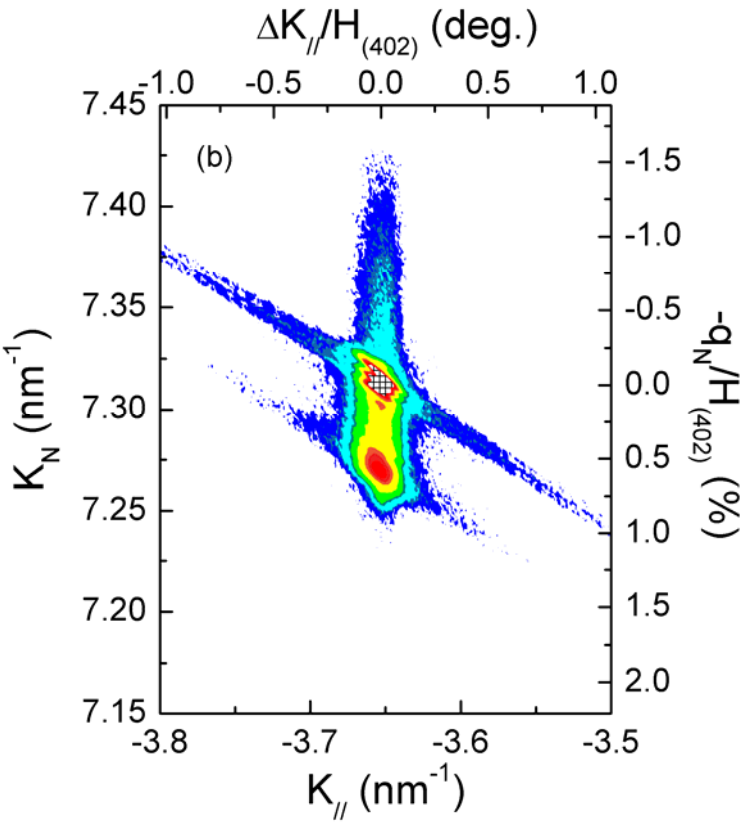
ΔK//H(402) (deg.)
-1.0
-0.5
0.0
0.5
1.0
(b)
7.45
7.40
7.35
7.30
7.25
7.20
7.15
KN (nm-1)
-1.5
-1.0
-0.5
0.0
0.5
1.0
1.5
2.0
-qN/H(402) (%)
-3.8
-3.7
-3.6
-3.5
K// (nm-1)

Figure 1(b)

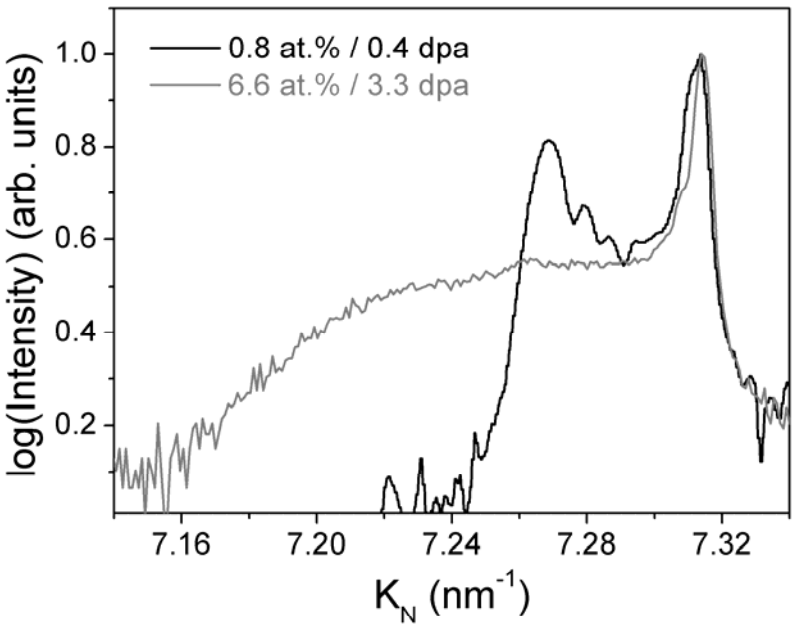
0.8 at.% / 0.4 dpa
6.6 at.% / 3.3 dpa
log(Intensity) (arb. units)
1.0
0.8
0.6
0.4
0.2
7.16
7.20
7.24
7.28
7.32
K_N (nm^-1)

Figure 2

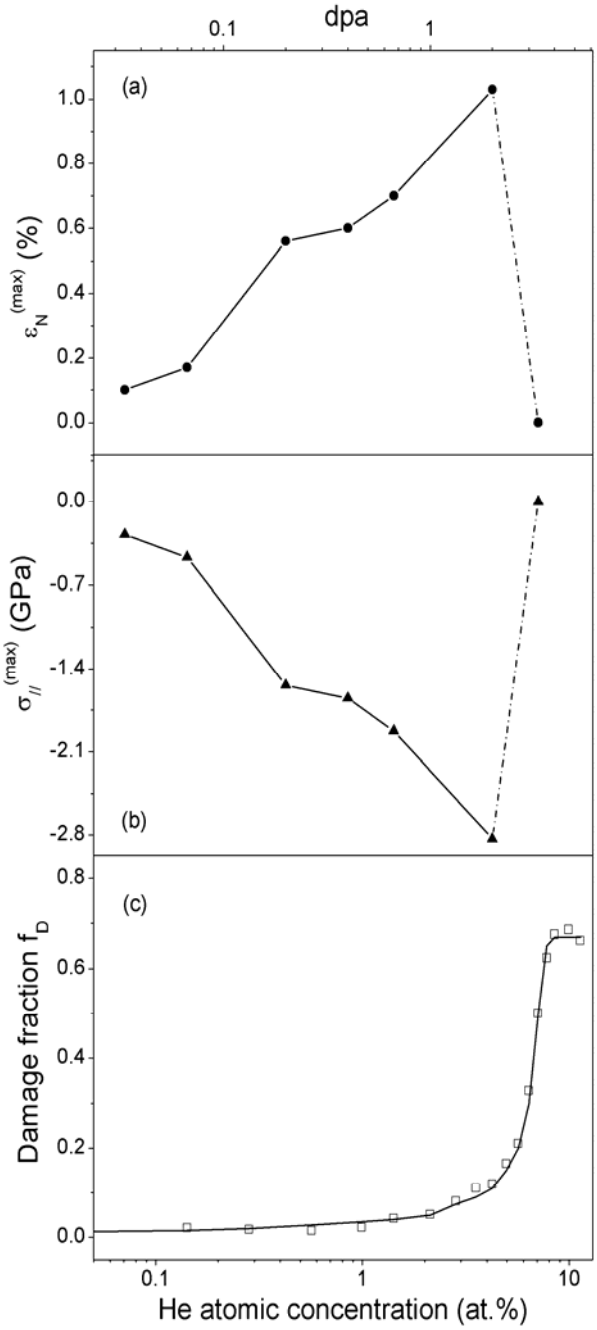
dpa
0.1
1
(a)
$\varepsilon_N^{(max)}$ (%)
1.0
0.8
0.6
0.4
0.2
0.0
(b)
$\sigma_{//}^{(max)}$ (GPa)
0.0
-0.7
-1.4
-2.1
-2.8
(c)
Damage fraction f_D
0.8
0.6
0.4
0.2
0.0
0.1
1
10
He atomic concentration (at.%)

Figure 3